Facile Fabrication of Lignin Crosslinked Hydrogel for Cationic Dye Adsorption and Antioxidant

Min Soo Kim, Ji Won Heo, Qian Xia, Do Hun Oh, Ji Woo Kim, and Yong Sik Kim *

*Corresponding author: yongsikk@kangwon.ac.kr

DOI: 10.15376/biores.19.3.5316-5337

GRAPHICAL ABSTRACT

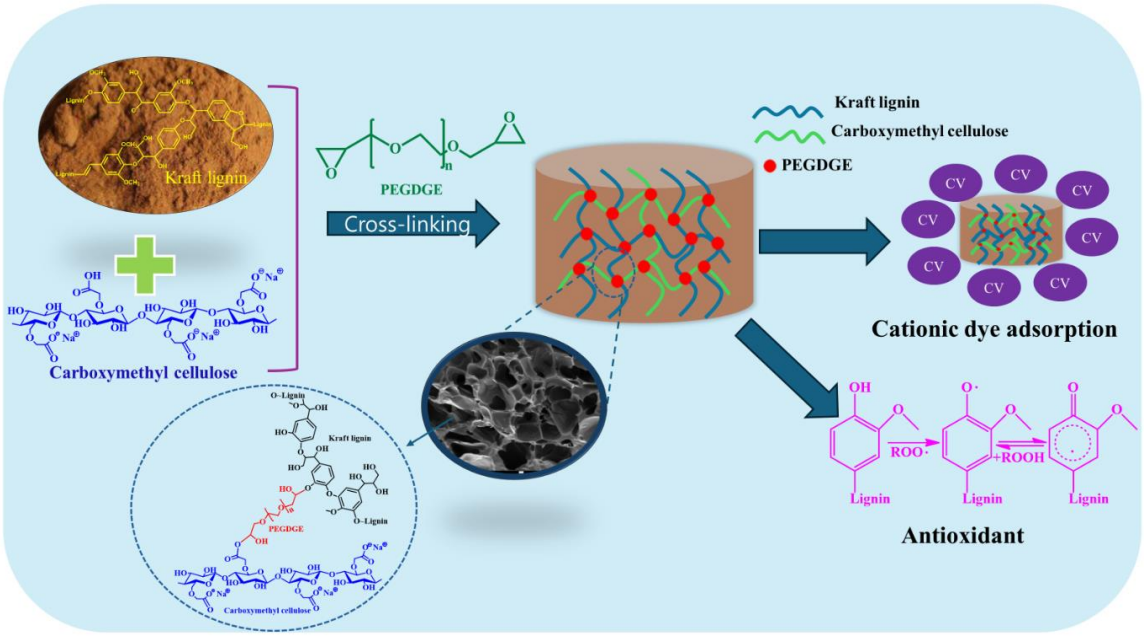

Facile Fabrication of Lignin Crosslinked Hydrogel for Cationic Dye Adsorption and Antioxidant

Min Soo Kim, Ji Won Heo, Qian Xia, Do Hun Oh, Ji Woo Kim, and Yong Sik Kim *

Lignin, renowned for its abundance of hydroxyl groups, was utilized in three dimensions to fabricate a hydrogel matrix. In this study, the optimal conditions for the preparation of a lignin-crosslinked hydrogel and its potential for dye and antioxidant removal were investigated. The hydrogel was synthesized through a cross-linking reaction, with varying amounts of cross-linking agent (poly(ethylene glycol) diglycidyl ether) added to adjust for the lignin content. Chemical structure analysis of the lignin-crosslinked hydrogel was conducted using Fourier-transform infrared spectroscopy and X-ray photoelectron spectroscopy, confirming successful hydrogel formation. Additionally, thermal analysis revealed an increase in the maximum thermal decomposition temperature with increasing cross-linker content. The lignin cross-linked hydrogel demonstrated a significantly higher swelling ability at pH 7 compared to pH 3. The dye adsorption capacity of the lignin-crosslinked hydrogel, which was evaluated using crystal violet (CV), showed a maximum adsorption capacity of 106 $mg \cdot g^{-1}$. The CV adsorption behavior followed Freundlich isotherms and pseudo-first-order kinetics. Moreover, the lignin-crosslinked hydrogel exhibited notable antioxidant activity, which was attributed to the phenolic hydroxyl groups of lignin macromolecules. Therefore, lignin-crosslinked hydrogels prepared using cross-linking agents have promising application potential in various fields.

DOI: 10.15376/biores.19.3.5316-5337

Keywords: Kraft lignin; Hydrogel; Antioxidant; Adsorption capacity

Contact information: Department of Paper Science and Engineering, College of Forest and Environmental Sciences, Kangwon National University, Chuncheon 24341, Republic of Korea;
**Corresponding author: yongsikk@kangwon.ac.kr*

INTRODUCTION

Lignin is an abundant component in the cell walls of plants. It is a complex organic polymer formed of monolignol units. Currently, lignin is generated as a by-product in the pulp and biorefinery industries. Its annual production reaches 100 million tons worldwide, but most of this amount is used as a low-cost fuel (Chen *et al.* 2020). Lignin has beneficial properties, such as antioxidant, antibacterial, biocompatibility, and UV protection (Koh *et al.* 2017). Lignin has several functional groups, including as aliphatic and aromatic hydroxyl, carboxylic acid, and ether bonds (Wang *et al.* 2014), and has a three-dimensional, crosslinked network structure (Lv *et al.* 2022). Meanwhile, due to its recalcitrance and complex structure, it is difficult to utilize compounds from lignin and to use it as a polymer material (Ragauskas *et al.* 2014). In the past decade, the utilization of lignin for value-added materials has been extensively sought after, since lignin valorization represents one of the main challenging issues of the paper industry and lignocellulosic biorefinery. In particular, the conversion of lignin into hydrogels shows great potential to

enhance lignin into high value-added materials.

A hydrogel is a hydrophilic polymer forming a three-dimensional network through the polymerization and crosslinking of one or more monomers (Akhtar *et al.* 2016; Rico-García *et al.* 2020). Hydrogels can retain a large amount of water in a swollen state within their network from surface tension and capillary forces (Zainal *et al*. 2021). Water adsorption by hydrogels depends on the functional groups and cross-linked network density of the hydrogel (Lim *et al.* 2017; Mahmud *et al.* 2018). Hydrogels also can exhibit excellent swelling capacity, shape, and compression resistance (Peppas *et al.* 2000). Hydrogels are used in sanitary products such as contact lenses, tissue engineering, wound dressing, or agriculture (Gennen *et al.* 2016). Synthetic polymers, formed by chemical reactions of small organic monomers, have been widely utilized for the construction of hydrogels (You *et al*. 2018). Although hydrogels based on synthetic polymers possess strong water adsorption and outstanding mechanical performances, they can suffer from poor biodegradability and potential toxicity (Zheng *et al.* 2017). In contrast, natural polymer-based hydrogel are of great interest due to their low cost, good biocompatibility, and biodegradability. In studies on biodegradable hydrogels, the primary raw materials include polypeptides, lignin, proteins, chitin, cellulose, starch, hemicellulose, chitosan, and gelatin (Cui *et al*. 2015, Murakami *et al.* 2010, Madl *et al*. 2016). Various technologies are required to effectively produce hydrogels using natural polymers.

Physical crosslinked hydrogels generally are held together by weak interactions such as hydrogen bonds (Dankers *et al.* 2005), ionic forces (Shim *et al*. 2005), hydrophobic forces, or van der Waals interactions (Brizzolara *et al.* 1996; Chung and Park 2009; Carafa *et al.* 2011). Physical crosslinked hydrogels have applications in a variety of fields. However, their mechanical strength is often regarded as inferior to that of chemically crosslinked hydrogels. Chemical crosslinked hydrogels are known to confer diverse properties, including enhanced mechanical strength facilitated by covalent bonding and crosslinking (Rico-García *et al.* 2020). These hydrogels are initiated by covalent crosslinking of polymer units by applying various strategies such as a low molecular weight crosslinking agent (Mao *et al.* 2020), crosslinked hybrid network (Lin *et al.* 2019), photosensitive crosslinker agent (Majcher *et al.* 2020), and so on. The crosslink points between polymer chains promote 3D network formation that affects the various physicochemical properties of the polymer incrementally by the crosslink density and the crystalline nature of the formed hydrogel structure (Karoyo *et al.* 2021).

Currently, research leveraging lignin's properties, such as its antioxidant and adsorption capabilities, is becoming increasingly diverse, and significant efforts are being made to explore the use of lignin in the development of hydrogels. Meng *et al*. (2019) reported that the production of hydrogels using lignin, which has properties such as antioxidant and biodegradability, can be used in various fields and has sufficient research value. According to Morales *et al*. (2020), a physically cross-linked hydrogel was prepared by adding lignin to PVA dissolved in NaOH solution and blending. From the viewpoint of hydrogel processing of lignin-based materials, independent gelation is still difficult due to the absence of an effective solvent system and the lack of rheological properties required for gelation (Jiang *et al.* 2020). Therefore, most lignin-based composite hydrogels are prepared through blending with various natural and synthetic polymers. Lignin, characterized by its abundance of hydroxyl groups, holds significant potential for the production of hydrogels through the use of epoxide-containing crosslinkers. Notable examples of such crosslinkers include epichlorohydrin (ECH), poly(ethylene glycol) diglycidyl ether (PEGDGE), and glycidyl methacrylate (Deng *et al.* 2008). Among these

candidates, PEGDGE stands out as a particularly promising candidate for facilitating the independent gelation of lignin. The gelation process involves the ring-opening reactions of PEGDGE's epoxy groups with the hydroxyl and carboxyl groups present in lignin, which can occur in both acidic and alkaline environments. This reaction forms robust three-dimensional networks. Nguyen *et al*. (2019) demonstrated that combining polyethylene glycol with PEGDGE produces hydrogels with superior chemical and physical stability. Therefore, the present work utilized PEGDGE, which contains diepoxide groups, to construct the hydrogel structure of lignin.

In this study, a hydrogel was prepared using PEGDGE as a cross-linking agent for the independent gelation of lignin. Additionally, the potential of the resulting lignin cross-linked hydrogel as an antioxidant and dye adsorption material was investigated. The chemical structure of the hydrogel was analyzed through Fourier-transform infrared spectroscopy (FT-IR) and X-ray photoelectron spectroscopy (XPS), and the physical properties were tested through thermogravimetric analysis (TGA). The swelling properties of KLH were measured under conditions of pH 3 and pH 7. Additionally, the total phenolic OH content was quantified using the Folin-Ciocalteu assay. Based on these results, the antioxidant capacity was evaluated using the 2,2-diphenyl-1-picrylhydrazyl (DPPH) assay. The characteristics and performance of the microcrystalline cellulose-based hydrogel (MCH) were then compared accordingly. Dye removal capacity was measured using a cationic dye crystal violet (CV).

EXPERIMENTAL

Materials

Kraft lignin (KL, M_n = 6,500 and M_w = 16,000 by GPC analysis, hydroxyl content = 4.2 mmol/g by ^{31}P NMR analysis) was provided from Tiger Forest and Paper Group Co., Ltds. The obtained lignin underwent additional purification through washing with deionized water (DW). The lignin was dewatered by filter-press and freezing drying. CMC (M_w = 250,000 g/mol, substitution of 0.9), PEGDGE (M_n =500 g/mol), ECH, Folin and Ciocalteu's phenol reagent, DPPH and CV were purchased from Sigma Aldrich (USA). Gallic acid, dimethyl sulfoxide (DMSO, 99.8%), methanol (99.9%) microcrystalline cellulose (MCC), sodium hydroxide (NaOH), potassium hydroxide (KOH, 98.0%) and urea were purchased Daejung Chemical (Korea). DW was prepared using a tertiary distillation device (HIQ II, Human Science, Korea). All purchased chemicals were used without further purification.

Preparation of Hydrogel (KLH)

The lignin-crosslinked hydrogel was prepared as shown in Fig. 1. KL (1 g) and 4% CMC solution (5 g) were placed in a 50 mL flask and sufficiently dispersed at room temperature for 1 hour using a magnetic stirrer (SL.SMS03038, DaiHan Scientific, Korea). Subsequently, 0.5, 1.0, 1.5, and 2.0 mmol of PEGDGE were added per 1 g of lignin, respectively, and stirred with a magnet for 30 min. Following stirring, the solution was transferred to glass vials and dried at 70 °C for 2 h using a drying oven (DH.SWOF07155, DaiHan Scientific, Korea). The dried samples were then subjected to several washes with 2 M HCl to remove any unreacted KL. This hydrogel was named kraft lignin crosslinked hydrogel (KLH). Based on PEGDGE dosage (0.5 mmol, 1.0 mmol, 1.5 mmol, and 2 mmol/g), the hydrogels were coded as KLH-1, KLH-2, KLH-3, and KLH-4, respectively.

For comparative purposes, MCC crosslinked hydrogel was prepared. MCC (4g) and NaOH/Urea solution were placed in a 100 mL flask with a magnetic stirring bar and distributed sufficiently at room temperature for 30 min. After stirring, the sample was completely frozen at 18 °C, followed by thawing. Then the sample were then thawed for approximately 2 h. ECH was added to the solution and stirred magnetically for 10 min. Subsequently, the solution was poured into glass vials and dried at 60 °C for 2 h.

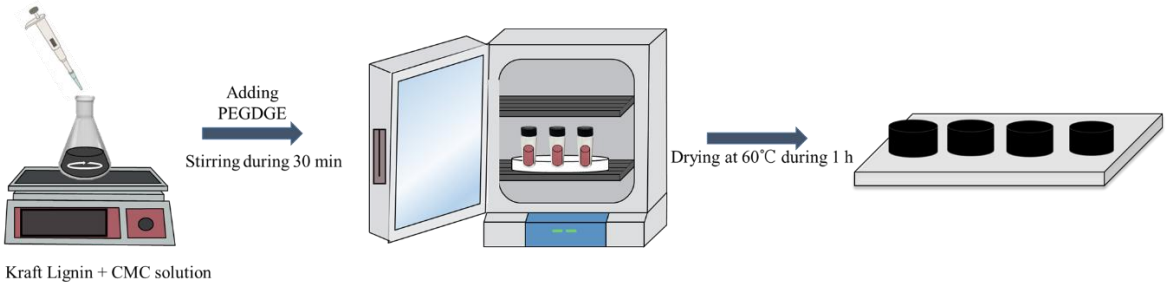

Fig. 1. Procedure for the preparation of KLH

Characterization of Hydrogel

In this study, lignin whose properties were analyzed through previous research was used (Zhang *et al*. 2023). The chemical structures of the hydrogel samples were analyzed by Fourier transform infrared (FT-IR) spectroscopy (Frontier, PerkinElmer, USA) in the attenuated total reflection (ATR) mode. The samples were measured at 25 °C and a spectral range of 4000 to 500 cm^{-1} at a resolution of 4.0 cm^{-1} with 64 scans (An *et al.* 2021b). Surface elemental analysis of the hydrogels was performed using X-ray photoelectron spectroscopy (XPS) (K-alpha+, Thermo Scientific, UK), and all samples were completely dried and made into aerogel form and analyzed (Fan *et al.* 2019). Analysis conditions were measured by scanning 30 times per sample with a dwell time of 30 ms and a passing energy 50 eV. Thermogravimetric analysis (TGA) for thermal properties of hydrogels was of hydrogels were conducted using a TA instrument (SDT Q600, USA) in the temperature range of 25 to 700 °C at a flow rate of 10 °C min^{-1} in a nitrogen atmosphere (An *et al.* 2020). The rheological properties of hydrogels were analyzed using a rheometer (HAAKE Viscostester iQ Rheometer, Thermo Fisher Scientific, Germany) with a parallel plate geometry (diameter 25 mm). The test was conducted immediately after stirring solution and adding the solution (0.5 mL) dropwise onto the plate. Before testing, hydrogel specimens for rheological tests were prepared by transferring 0.5 mL of the reaction mixture into a disk-shaped mold, heating to a temperature of 80 °C for 20 min, and then cooling the gel in the mold to 25 °C for 20 min (Teng *et al.* 2017). The measurement was performed to measure G' and G'' of the hydrogel with shear frequency in the range of 0.1 to 20 Hz at room temperature. To investigate the morphology, images were obtained using a scanning electron microscope plus and energy X-ray spectroscopy (SEM-EDS) (EVO-LS10, Zeiss, Germany).

To confirm the swelling characteristics of the prepared hydrogel, measurements were conducted after adjusting the pH to 3 and 7 using HCl and DW. Each sample was run for a total 24 h. Before the swelling, each sample were dried in a freeze dryer (FDB-5503, OPERON, Korea) at -50 °C to change aerogels. The swelling percentage was calculated using Eq. 1 as follows:

$$Swelling\ ratio\ (\%) = \frac{W_s - W_d}{W_d} \times 100 \quad (1)$$

The weight of aerogels (W_d) was measured using a Sartorius balance. The wet weight of samples (W_s) was measured at consecutive time intervals for 6 h. Before weighing, each sample was dried by removing water from the surface using tissue paper.

To assess the degree of KL involvement in the cross-linking reaction relative to the quantity of added PEDDGE, measurements were performed to determine the conversion rate of KL and the cross-linking density of the prepared hydrogel. Each test was performed in triplicate. The conversion efficiency was calculated using Eq. 2 as follows,

$$Y\% = (m_i - m_w)/m_i \times 100 \quad (2)$$

where Y is the conversion efficiency of KL after the crosslinking reaction, m_i is the initial amount of KL added in the crosslinking reaction, and m_w is the amount of KL in the washing water (Teng *et al.* 2017).

A UV spectrometer was used to measure the residual KL in the washing water due to its characteristic absorbance at a wavelength of 280 nm. Kraft lignin was dissolved by concentration up to (4 to 20) μg ·mL^{-1} using 3.3 M KOH. Lignin samples were measured by UV spectrometer at different concentrations. A calibration curve was established using the values measured at 280 nm and then used to calculate the mass of the residual KL in the extraction water (Chen *et al.* 2016). The gel content was calculated using Eq. 3 as follows,

$$X\% = m_a - m_b \times 100 \quad (3)$$

where X is the gel content of KL, m_a is the weight of the aerogel after washing, and m_b is the weight of the aerogel before washing (Teng *et al.* 2017).

To assess the success of cross-linking between lignin and PEGDGE, total phenolic hydroxyl group measurements were performed. The total phenolic content of the KLH samples was determined as gallic acid equivalent using the Folin-Ciocalteu method. The gallic acid in DMSO solution (with six different concentrations from 0 to 20 μg·mL^{-1}) was used to construct a standard calibration curve (R^2 > 0.99). All solutions were freshly prepared and immediately used. KLH samples were processed as follows. Each sample was prepared at a concentration of 20 mg·mL^{-1} by dissolving it in DMSO. Subsequently, 2 mL of KLH the solution, along with 2 mL of Folin-Ciocalteu's reagent and 1 mL of Na_2CO_3 (15% w/v) were mixed and shaken for 60 min in darkness (An *et al.* 2021a). The resulting mixture was diluted by bringing the volume to 10 mL with distilled water. The absorbance of the solution was measured at 765 nm using a UV-Vis spectrometer. The total phenolic OH content of the KLH samples was calculated based on the obtained absorbance values (Zhang *et al.* 2023a).

To ascertain whether the free radical scavenging capability of lignin persists even in the gel state, antioxidant evaluation was conducted using DPPH. The KLH samples were dispersed in DMSO, followed by mixing the sample suspension with a 0.15 mM DPPH-methanol solution in the same ratio in a tube. The tube was covered with aluminum foil to protect against light penetration and then incubated in a shaking incubator (IST-4075, JEIO Tech, Korea) at 200 rpm for 30 min with shaking at 25 °C. Subsequently, the absorbance of the mixture was recorded at 517 nm using a UV-Vis spectrometer (UV-2550, Shimadzu, Japan) (Heo *et al.* 2023). A minimum of three experiments was conducted for each sample to calculate the mean and standard deviation. The radical scavenging capacity (RSC, %) of the sample was calculated using Eq. 4 as follows,

$$RSC\ (\%) = \frac{A_{control} - (A_{sample} - A_{blank})}{A_{control}} \times 100 \quad (4)$$

where $A_{control}$ is the absorbance of the equal-ratio mixture of DMSO and DPPH-methanol solution, A_{sample} is the absorbance of the equal-ratio mixture of sample suspension and DPPH-methanol solution, and A_{blank} is the absorbance of the equal-ratio mixture of sample suspension and methanol (Heo *et al.* 2023).

To evaluate the cationic dye adsorption capacity of the prepared hydrogels, measurements were performed using CV. Solution of CV with a concentration of 200 $mg \cdot L^{-1}$ was prepared. KLH-2 (50 mg) was mixed with a dye solution (30 mL) in Erlenmeyer flask, with different pH ranges of (3 to 10), and then dye adsorption was carried out in a shaking incubator for different times (0 to 24 h) at 25℃. The concentration of CV was confirmed with UV spectroscopy (UV-2550, Shimadzu, Japan) at a maximum wavelength, respectively. (CV: 592 nm). The adsorption efficiency E (%) and adsorption amounts Q ($mg \cdot g^{-1}$) at equilibrium were determined according to the Eqs. 5 and 6, respectively,

$$E\ (\%) = \left[(C_i - C_f)/C_i\right] \times 100 \quad (5)$$

$$Q\ (mg \cdot g^{-1}) = \left(C_i - C_f\right) \times V/M \quad (6)$$

where C_i and C_f are the initial and final dye concentrations in the solution ($mg \cdot L^{-1}$), respectively; V is the volume (L) of the CV solution, and M is the weight (g) of the adsorbent (Heo *et al.* 2022).

RESULTS AND DISCUSSION

Characterization of KLH

Chemical structures of KLH

The surface elemental composition and chemical structure of KL and KLH samples were evaluated using XPS. Figure 2(a) presents the XPS survey scan spectra of KL and KLH-4. In Fig. 2(a), two major peaks corresponding to C1s (283 eV) and O1s (531 eV) were observed for all samples (Bañuls-Ciscar *et al.* 2016). The C1s core-level spectra of KL and KLH-4 are shown in Fig. 2(b-c), respectively. Two peaks can be deconvoluted at 283 and 285 eV, which account for the C–C/C=C and C–O bonds, respectively. In Fig. 2(c), the binding energies at 283, 285, and 287 eV belong to the C–C/C=C, C–O, and C=O bonds, respectively, which indicates the formation of a cross-linked network in hydrogel (Adolfsson *et al.* 2015).

The chemical functional groups of KLH were analyzed using FTIR analysis. The FT-IR spectra of raw material and KLH are shown in Fig. 3(a-b). In Fig. 3(a), characteristic peaks at 850, 1097, and 2868 cm^{-1} corresponded to the –CH, C–O–C, and –CH bonds of PEGDGE, respectively (Teng *et al.* 2017). In the other spectrum, characteristic peaks of CMC were observed at 1588 cm^{-1} (assigned to the O=C–O–(H)), 1322 cm^{-1} (assigned to the O-H bonding), and 1020 cm^{-1} (assigned to the R–O–R). Additionally, characteristic peaks of KL were observed at 3393 cm^{-1} (assigned to the O–H bonding) and 1240 cm^{-1} (assigned to the C–O(H)). An aromatic ring peak was confirmed at 1400 to 1500 cm^{-1} (Yue *et al.* 2011).

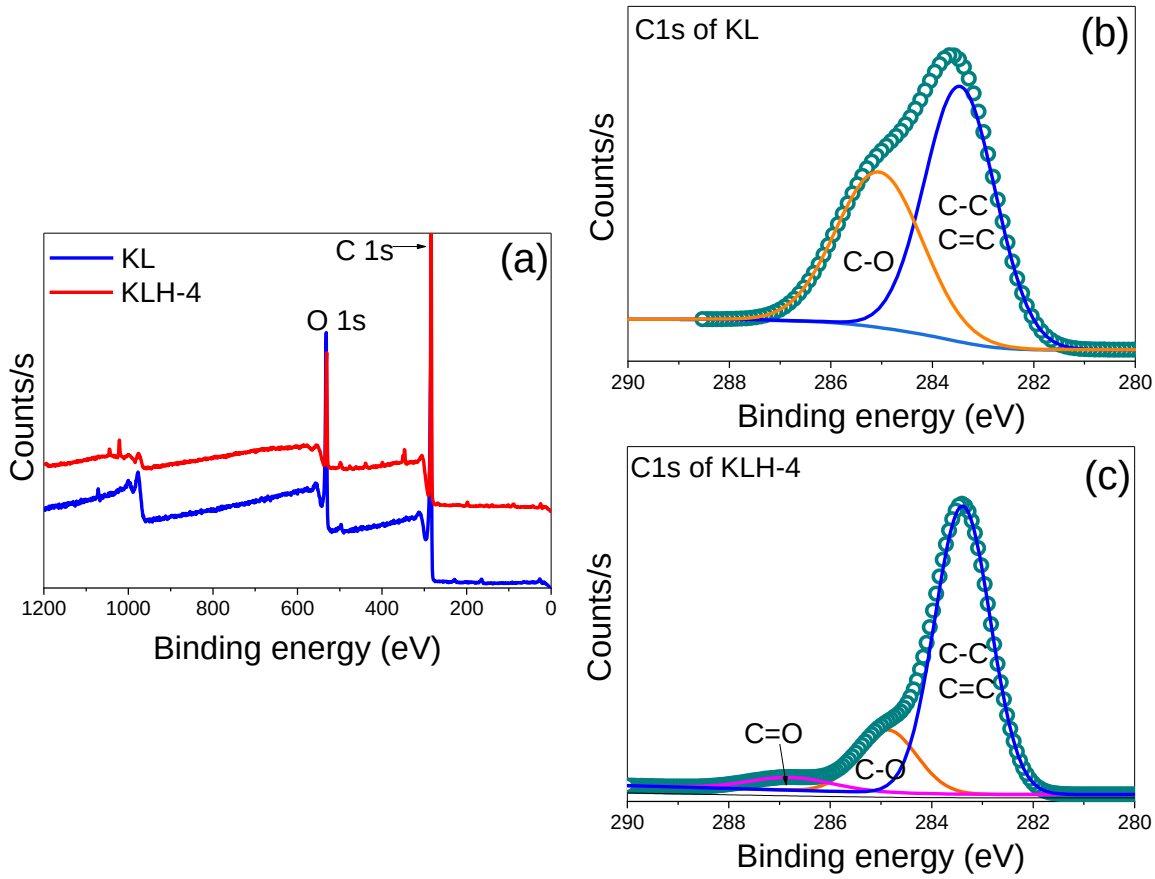

Fig. 2. (a) XPS survey scan spectra, (b-c) C1s core level spectra of KL and KLH-4

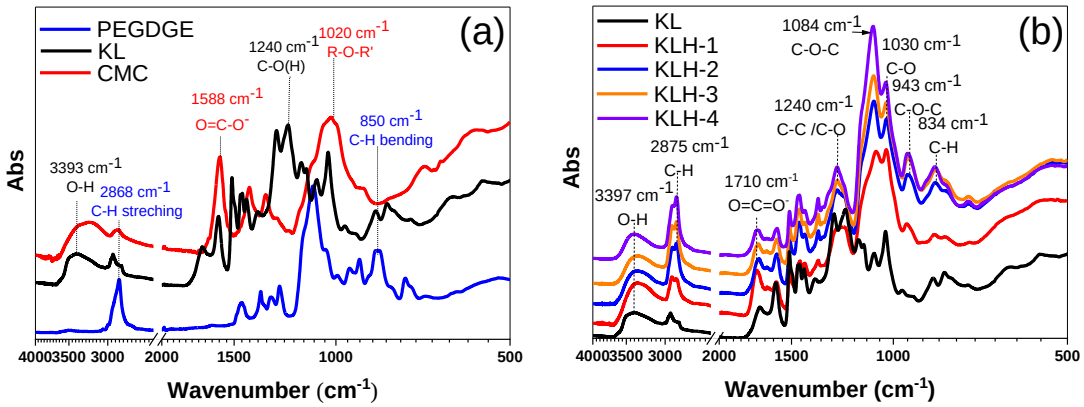

Fig. 3. (a) FTIR spectra of KL, CMC, PEGDGE and (b) FTIR spectra of KLH samples

In the FTIR measurement results after hydrogel preparation, Fig. 3(b), the characteristic peaks at 2868, 1083, and 1030 cm^{-1} corresponded to the C–H, C–O–C, and C–O bonds of KLH, respectively. The increase in the peak that appears around 2800~2900 cm^{-1} belongs to the C–H stretching of methylene in PEGDGE (Yoo *et al.* 2019) Additionally, the presence of PEG segments in the hydrogel was supported by specific peaks in KLH at 1084 and 1030 cm^{-1} corresponding to C–O and C–O–C stretching vibrations. Compared with the PEGDGE, the 843 cm^{-1} peaks assigned to the epoxy group

decreased in KLH. Simultaneously, the peak of KLH at 1240 cm^{-1} which originated from phenolic –OH stretching of pristine lignin also decreased. Through the results of specific peaks, it was confirmed that the epoxide presents in PEGDGE reacted with the phenolic OH of lignin through ring opening. The peak observed around 3400 cm^{-1} was confirmed to be the –OH peak present in KL, and the peak observed around 1500 to 1600 cm^{-1} was identified as the characteristic aromatic ring peak of KL. Additionally, it was confirmed that the peak appearing at 1710 cm^{-1} corresponds to the O=C–O–(H), which is one of the specific peaks of CMC. The FTIR spectra illustrated the presence of KL or CMC in KLH hydrogels and the successful preparation of KLH *via* the crosslinker PEGDGE (Dai *et al.* 2020).

TGA, Gel Content, and Rheological Properties of KLH

TGA was performed to determine the thermal properties of the KLH samples. TGA curves and derivate thermogravimetry (DTG) of KLHs are shown in Fig. 4(a). In the DTG graph, a three-stage decomposition was achieved (Li *et al.* 2018; Tian *et al.* 2018). The slight weight loss observed below 100 ℃ in all the KLH samples was attributed to the gradual evaporation of water. Decomposition of CMC used as an auxiliary agent occurred in all KLH samples around 200 to 300 ℃ (Akar *et al.* 2012; Scarica *et al.* 2018). Over 300 to 400 ℃, the decreases in mass showed the decomposition of crosslinked lignin by PEGDGE (Guo *et al.* 2018). As the amount of PEGDGE added increased, the temperature at which the KLH samples thermal decomposition increased (Cortés-Triviño *et al.* 2018). The introduction of the PEGDGE moiety into lignin was confirmed to enhance thermal decomposition. As a result of checking the maximum thermal decomposition temperature, KL was 264 ℃, while KLH-4 exhibited an increase of 325 ℃. These results confirmed that the maximum thermal decomposition temperature of the KLH sample increased as the amount of PEGDGE added increased. The maximum thermal decomposition temperature and thermal stability increase as the amount of crosslinking agent added increases, due to the enhancement of bonding and structural stability between lignin molecules. In addition, it was confirmed that when PEGDGE was added above a certain level, the PEGDGE moiety increased, and the amount of thermal decomposition increased.

Figure 4(b) shows the conversion of KL and gel content of KLH samples, depending on the amount of cross-linker added. Gel content is one of the properties required for hydrogel experiments because it can determine the crosslinking density of the produced hydrogel. In addition, the amount of lignin used in the crosslinking reaction during gel production was also measured. As a result of measuring the gel content, it was confirmed that the KLH sample was generally more than 95%. As the amount of PEGDGE added increased, the bonding between lignin molecules increased and the gel content increased. In addition, the conversion of KL also showed a tendency to increase the amount of KL used in the crosslinking reaction as the amount of PEGDGE added increased.

Figure 4(c-d) shows G' (storage modulus) and G'' (loss modulus) about KLH. Rheological properties are crucial for the prepared hydrogel, and by measuring G' and G'', it is possible to determine the dominant viscoelastic behavior of the hydrogels. Both G' and G'' of hydrogels increased with vibration frequency but reached equilibrium above a certain point, indicating typical viscoelastic behavior (Zerpa *et al.* 2018). G' was higher than G'' over the whole range of frequencies, suggesting a general dominance of the elastic response of the gels to deformation over a broad time scale (Passauer 2012; Zerpa *et al.* 2018). In Fig. 4(c), KLH-2 showed the highest value. In the case of KLH-1 and KLH-2, G' and G'' values tended to increase as the amount of PEGDGE added increased. KLH-3 and KLH-4

showed lower results than KLH-1 due to the increased flexibility of the PEG chains from higher PEGDGE ratio with the more crosslinking agent. As a result of comparing *G′* and *G″* values from the rheological properties, it was found that KLH is a hydrogel with superior elastic properties over viscous properties.

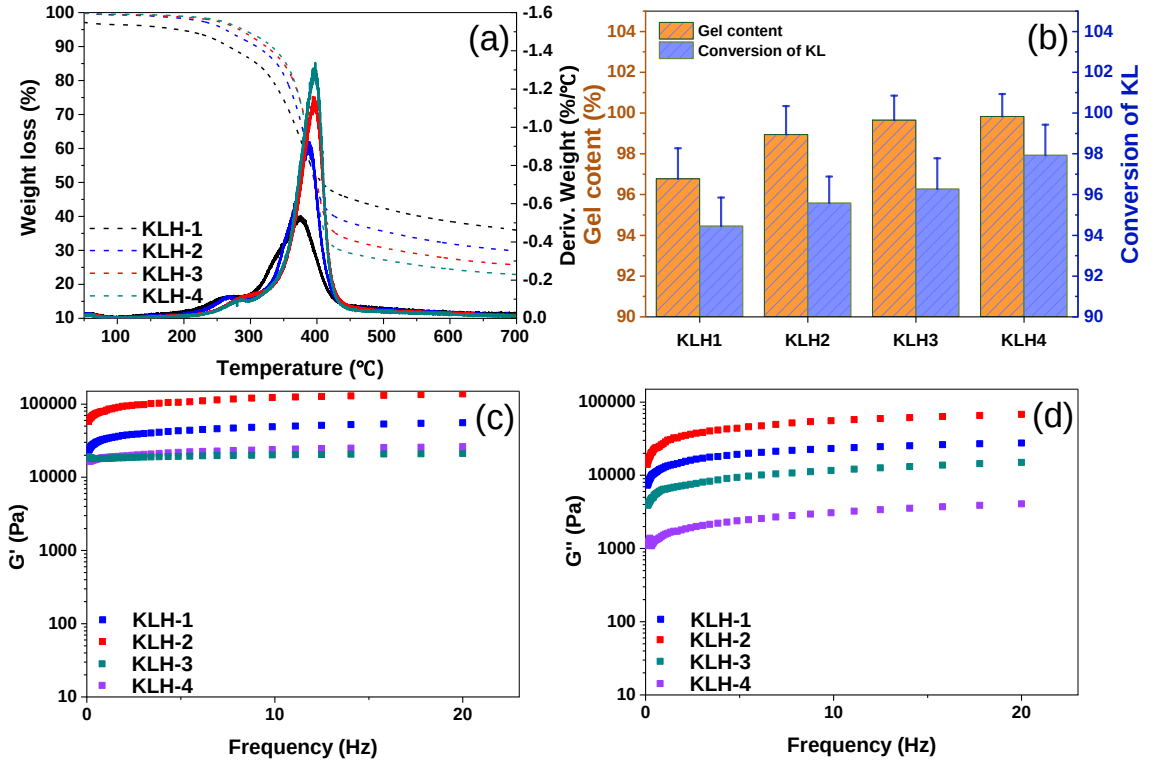

Fig. 4. (a) TGA and DTG curves of thermal decomposition for KL and KLH, (b) gel content and conversion of KL, (c-d) storage modulus and loss modulus of KLH

Swelling and interior morphology of KLH

The swelling properties of hydrogels are an important parameter affecting the use of hydrogels. The measurement data of the swelling rate for this are shown in Fig. 5. Hydrogel can retain a large amount of water molecules when immersed in a water environment regardless of pH. KLH shows a swelling degree of 220 to 250% at pH 3. On the other hand, as pH increased, the swelling degree also increased, eventually reaching 250 to 310% at pH 7. The reason is the specific structure of lignin, which contains a large number of polar groups such as aromatic and aliphatic hydroxyl groups (Ciolacu and Cazacu 2018). In general, lignin possesses both aromatic and aliphatic hydroxyl groups, resulting in a characteristic negative surface charge that increases with rising pH. The negative charges generated by these properties induce repulsion between lignin particles, leading to the expansion of the three-dimensional network and ultimately facilitating the penetration of more water molecules. KLH-1 showed the best swelling rate in both pH 3 and pH 7, and the swelling rate tended to decrease as the amount of crosslinking agent added increased.

Due to the small amount of cross-linking agent added to KLH-1, a higher proportion of phenolic hydroxyl groups remain uncrosslinked compared to other samples. These remaining phenolic hydroxyl groups result in electrostatic repulsion between lignin particles and enhance the penetration of water molecules (Ciolacu *et al.* 2012; Thakur and

Thakur 2015). As the amount of crosslinking agent increased, the swelling ratio decreased due to reduced space for water molecules to penetrate, resulting from stronger binding between lignin particles.

Based on the comprehensive analysis findings of KLH, it has been established that KLH-2 embodied the optimal production conditions for lignin-crosslinked hydrogels. KLH-1 had the highest swelling percentage but lacked shape retention compared to other samples. In addition, KLH-3 and KLH-4 also had reduced swelling degree due to strong crosslinking, and their rheological properties also showed lower values than KLH-1. In conclusion, KLH-2 was judged to be the optimal production condition for lignin-crosslinked hydrogel through chemical analysis, swelling, and rheological property analysis.

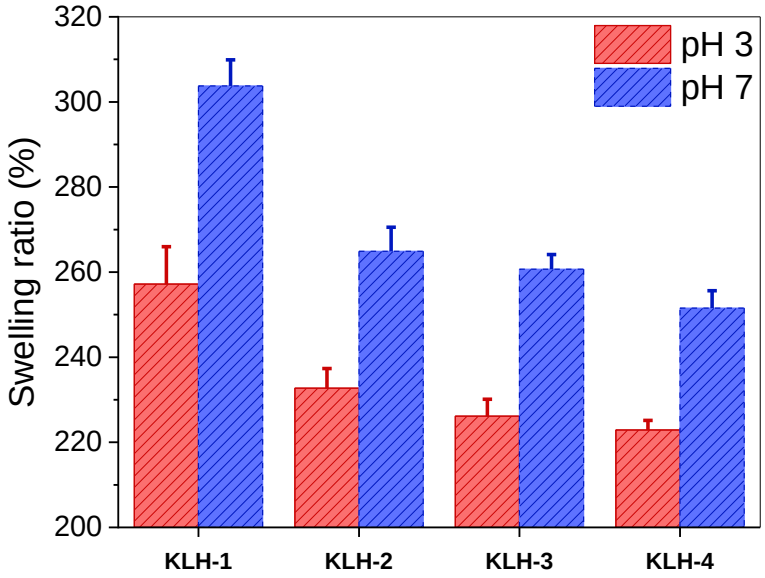

Fig. 5. Swelling ratio of KLHs with different pH conditions

Figure 6 shows the internal morphological structure of KLH. The images confirmed that the KLH samples had a porous structure. The introduction of polyethylene glycol segments into this configuration resulted in the formation of a porous structure, which can be attributed to the establishment of a network structure or three-dimensional crosslinking. In the KLH sample, an increase in the amount of crosslinking agent resulted in thicker pore-forming regions. This phenomenon was attributed to the enhanced bonding between lignin particles, leading to a denser network structure with the increased crosslinking agent. However, it is difficult to control the size or shape of the pores inside the hydrogel. Therefore, additional research is needed to control tunable or uniform pores.

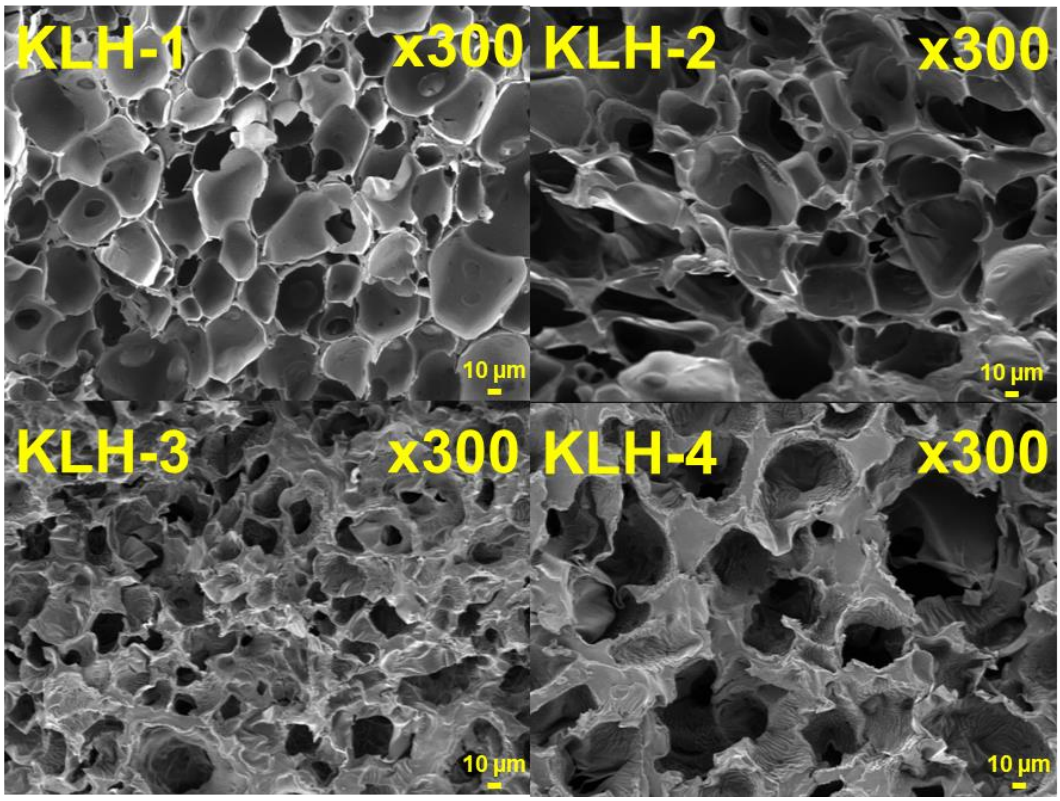

Fig. 6. SEM images of KLH samples

Total phenolic OH content and antioxidant of KLH

The measurement of total phenolic hydroxyl groups was conducted to ascertain the success of cross-linking between lignin and PEGDGE, as well as its impact on antioxidant properties. The phenolic OH content of the hydrogel varied depending on the degree of crosslinking and is summarized in Table 1. The OH content in KL was initially the highest and decreased with the increasing addition of the crosslinker. This observation confirmed the successful cross-linking between lignin and PEGDGE, specifically indicating that the phenolic hydroxyl group of lignin actively participates in the ring-opening reaction with PEGDGE.

To evaluate whether the antioxidant properties of lignin, specifically its ability to scavenge free radicals, are retained in the hydrogel state, an antioxidant assessment using DPPH was performed. Figure 7 presents the antioxidant capacities of the KLH samples. The antioxidant activity of KLH was found to be closely associated with the level of phenolic hydroxyl groups, which play a critical role in this process (Piccinino *et al.* 2021; Sheng *et al.* 2022). Among the samples, KLH-1 exhibited the highest antioxidant activity. As the amount of cross-linking agent increased, a greater number of cross-linking reactions occurred, leading to a reduction in the phenolic hydroxyl groups in lignin and a consequent decrease in antioxidant activity. To provide a comparative analysis, an MCC-based hydrogel was also prepared, and its antioxidant capacity evaluated. Compared to KLH-4, which contained the highest amount of cross-linking agent, the MCC hydrogel exhibited more than twice the reactive oxygen species scavenging ability. In conclusion, the antioxidant properties of the KLH samples were confirmed, with an active oxygen removal capacity exceeding 80%, indicating a significantly higher performance compared to the MCC hydrogel.

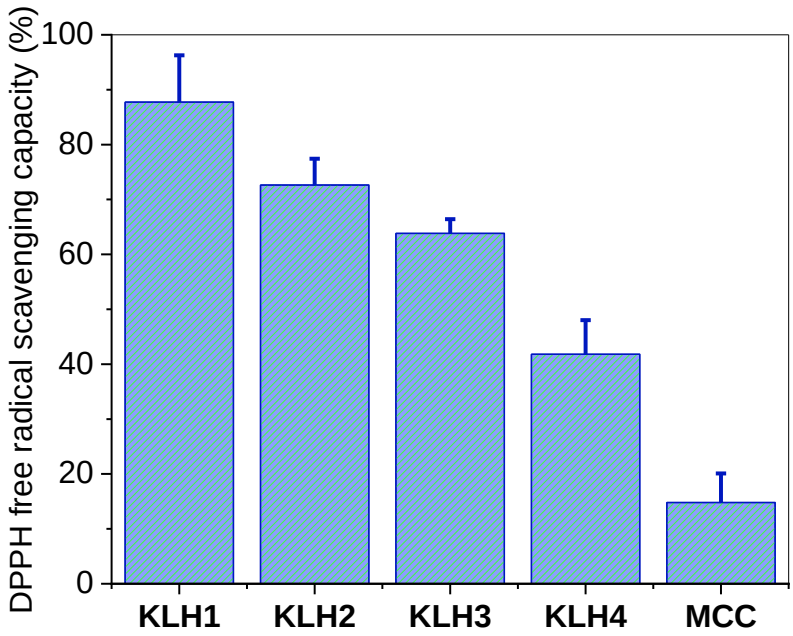

Fig. 7. DPPH free RSC of KLH samples and MCH

Table 1. Total Phenolic OH Content of KLH Samples and MCH

Sample	Phenolic OH content
	mmol·g^{-1}
KL	1.283
KLH-1	0.343
KLH-2	0.127
KLH-3	0.069
KLH-4	0.066
MCH	0.011

Effect of Dye Adsorption of KLH

Effect of adsorption time and pH on the removal efficiency

The comparative adsorption capacities for the CV of each sample are shown in Fig. S1. Among the samples, KLH-2 was confirmed to have the highest adsorption capacity. Based on this result, subsequent adsorption capacity measurements were conducted exclusively using KLH-2. Figure 8(a) shows various adsorption times with respect to CV removal efficiencies of the KLH-2. The experiment was carried out from 0 to 1440 min, adsorption amount gradually increased from 0 to 240 min, after 240 min, the equilibrium was achieved to confirm the adsorption percentage of 90% or more. At 1440 min, an adsorption of about 90% was confirmed, but a decreasing trend was confirmed.

pH is an important influencing factor in adsorption *via* the ionization of the dye or the functional groups of the adsorbent. The adsorption with a KLH-2 sample from pH 2 to 10 are shown in Fig. 8(b). The adsorption rate of 90% or more appeared without significant change depending on the pH. Because KLH samples is basic, the adsorption rate was expected to increase as pH increased, but there was no significant change in the adsorption rate despite the pH change.

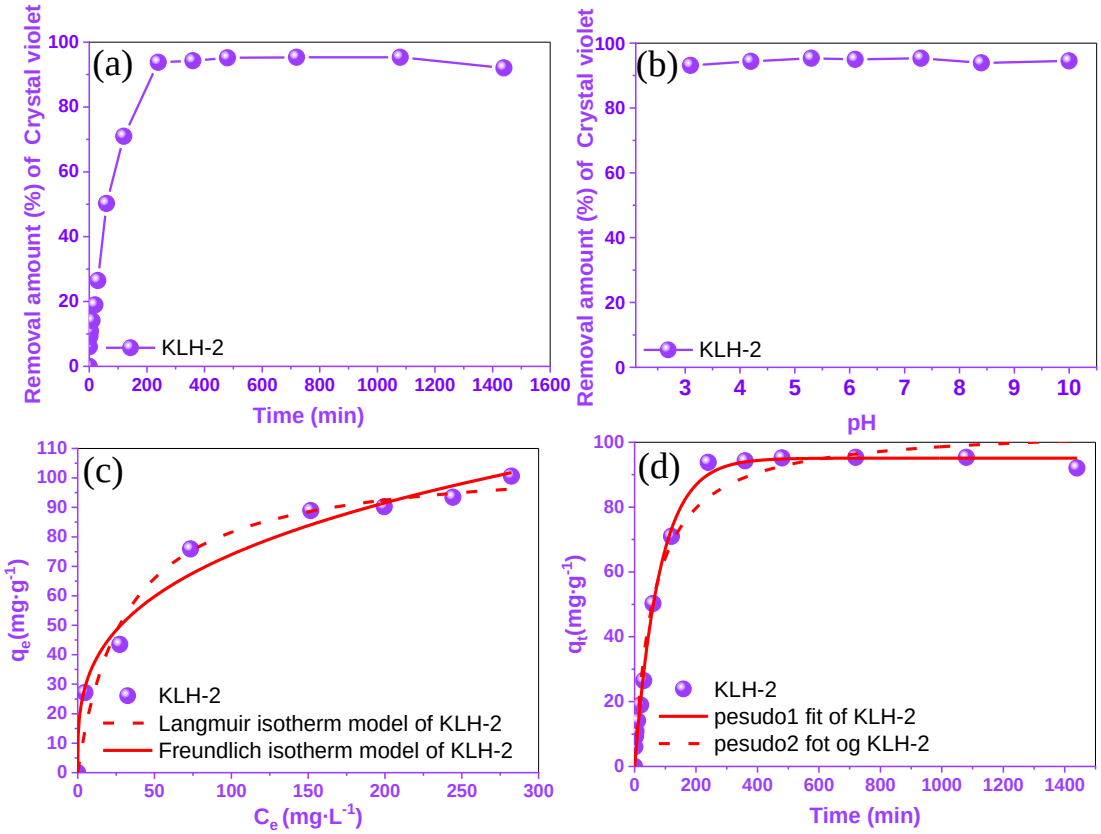

Fig. 8. (a) Effect of contact time on the removal amount of CV, (b) effect of pH on the removal amount of CV, (c) nonlinear fitting curves of isotherm models (Langmuir and Freundlich models) for the adsorption of CV onto KLH, (d) nonlinear fitting curves of kinetic models (pseudo-first-order and pseudo-second-order kinetic models) for the adsorption of CV onto KLH

Analysis of CV Adsorption Isotherms and Kinetics

CV adsorption isotherms

Adsorption isotherms were obtained based on the effect of the initial adsorbent concentration on the adsorption capacity. The adsorption experiment was fixed at pH 6 and 25 °C for each concentration. Langmuir and Freundlich adsorption isotherms were used to match the adsorption isotherms. The nonlinear Langmuir and Freundlich equations are represented by Eqs. 7 and 8, respectively,

$$q_e = \frac{q_m k_L C_e}{1+k_L C_e} \quad (7)$$

$$q_e = k_F C_e^{\frac{1}{n}} \quad (8)$$

where q_e is the equilibrium adsorption capacity (mg·g^{-1}), C_e is the concentration of the adsorbate at equilibrium (mg·L^{-1}), q_m is the maximum adsorption capacity (mg·g^{-1}), k_L is the Langmuir constant, k_F is the multilayer adsorption capacity, and n is an empirical parameter related to the intensity of adsorption (Chatterjee *et al.* 2010; Olusegun and Mohallem 2020).

Figure 8(c) shows the experimental data fitting for Langmuir and Freundlich isotherm models. Related nonlinear equation parameters are listed in Table 2. KLH-2 had a higher correlation coefficient of the Freundlich isotherm model than the Langmuir isotherm model. The results confirmed that equilibriums were better described by the Freundlich isotherm models at 25 °C.

Table 2. Characterization Parameters of Adsorption Isotherms for the Adsorption of CV onto KLH

Isotherms	Parameters	CV
		KLH-2
Langmuir isotherm	R^2	0.75
	k_L (L·mg^{-1})	0.032
	$q_{m(cal)}$ (mg·g^{-1})	106.82
Freundlich isotherm	R^2	0.983
	k_F (mg·g^{-1})	17.95
	n	0.307

CV adsorption kinetics

The adsorption kinetics were determined based on the effect of the adsorption time on the adsorption capacity. The common mathematical models: pseudo-first- order and pseudo-second-order kinetic models were used to fit the adsorption kinetics data. The nonlinear pseudo-first-order and pseudo-second-order kinetics equations are given in Eqs. 9 and 10, respectively,

$$q_t = q_e (1 - e^{-k_1 t}) \quad (9)$$

$$q_t = \frac{q_e^2 k_2 t}{1 + q_e k_2 t} \quad (10)$$

where q_e is the equilibrium adsorption capacity (mg·g^{-1}), q_t is the adsorption capacity (mg·g^{-1}) at time t (min), and k_1 and k_2 are the kinetics rate constants for pseudo-first-order and pseudo-second-order kinetic models, respectively (Dinu and Dragan 2010; Zhang *et al.* 2011).

Based on the experimental data obtained from the effect of the settling time on the removal amount, the data were fitted using pseudo-first-order-and pseudo-second-order dynamic models, as shown in Fig. 8(d). The equation parameters are listed in Table 3. The coefficient of determination of the pseudo-first-order kinetic model was higher than that of the pseudo-second-order kinetic model. Thus, KLH is more suitable for similar first-order kinetics with adsorption to CV. This result determined that since KLH is in the form of a hydrogel and crosslinking between lignin is formed, physical adsorption would be performed rather than chemical adsorption, and the result was confirmed to be suitable. Nguyen *et al*. (2022) utilized a gellan gum/bacterial cellulose gel to adsorb crystal violet (CV) and reported an adsorption capacity of 17.6 mg/g. Similarly, Truong *et al*. (2019) developed a cellulose-based hydrogel that adsorbed methylene blue, demonstrating an adsorption capacity of 41.7 mg/g. Comparing these results with other studies on natural polymer-based hydrogels, it was confirmed that the lignin cross-linked hydrogel prepared in this study possesses sufficient functionality as an adsorption material.

Table 3. Characterization Parameters of Adsorption Kinetics for the Adsorption

Isotherms	Parameters	CV
		KLH-2
Pseudo-first-order	R^2	0.994
	K_1 (x10^{-2}) (g·mg^{-1}·min^{-1})	0.012
	$q_{e(cal)}$ (mg·g^{-1})	95.10
Pseudo-second-order	R^2	0.983
	K_2 (x10^{-3})(min^{-1})	1.51
	$q_{e(cal)}$ (mg·g^{-1})	104.84
	$q_{e(exp)}$ (mg·g^{-1})	114.42

Possible Mechanism

Lignin possesses numerous aromatic rings and a complex three-dimensional structure. In this study, more network structures were constructed to utilize cross-linked lignin-based hydrogels as superior adsorbents for cationic dyes. The adsorption mechanism of crystal violet (CV) using KLH is depicted in Fig. 9.

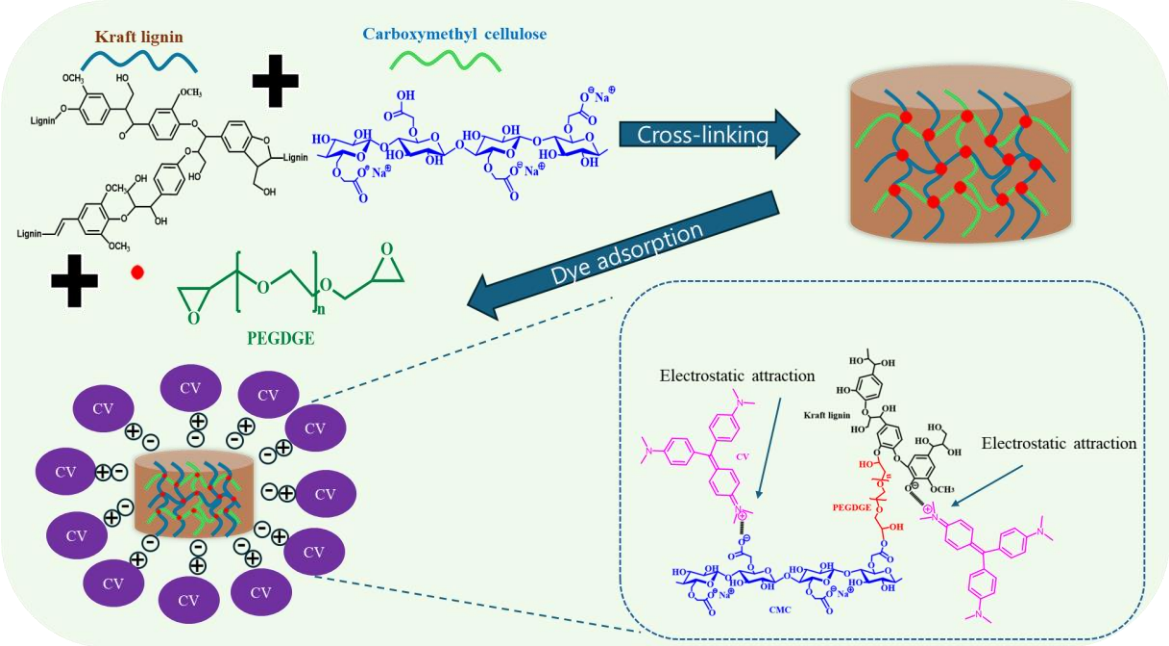

Fig. 9. Possible adsorption mechanism of CV on KLH

The KLH adsorbent effectively removes cationic dyes due to the chemical characteristics of lignin. KLH exhibited a negative surface charge due to its phenolic hydroxyl groups, resulting in electrostatic attraction with the cationic dye CV. The chemical structures of CV and lignin include aromatic rings, facilitating the dye's approach to the adsorbent surface through π-π interactions (Heo *et al*. 2022). Additionally, the network structure of KLH, with PEG segments between lignin molecules, increases the number of reactive sites available for the dye and enhances adsorption efficiency. Thus, KLH adsorbent exhibits a synergistic effect by promoting greater adsorption through chemical interactions with the dye and the porous structure within the hydrogel.

CONCLUSIONS

1. A lignin-based hydrogel was prepared using poly(ethylene glycol) diglycidyl ether (PEGDGE) for independent gelation of lignin, and the change in physical properties according to the amount of PEGDGE added was studied. It was confirmed that kraft lignin hydrogel (KLH) was successfully manufactured through physical and chemical analysis of KLH.
2. KLH exhibited predominant elastic properties, thereby ensuring the maintenance of mechanical stability.
3. The antioxidant properties of KLH were found to be at least twice as effective as those of the comparison group, microcrystalline cellulose hydrogel (MCH). This result confirms the potential of KLH as an antioxidant material.
4. KLH was shown to be suitable for the Freundlich model and a pseudo-first-order model, which means that KLH exhibits multilayer adsorption behavior. This observation confirms the potential of KLH as an effective adsorption material.
5. In conclusion, this study demonstrated the feasibility of fabricating lignin-based hydrogels with confirmed antioxidant properties and dye removal capabilities. It suggests that lignin can be fully utilized as a hydrogel material with tailored properties, highlighting its potential for high-value applications and its significant contribution to research in this field.

ACKNOWLEDGMENTS

This work was supported by the National Research Foundation of Korea (NRF) grant funded by the Korea government (MSIT) (2021R1A2C2008178), and the Ministry of Education (2018R1A6A1A03025582).

REFERENCES CITED

Adolfsson, K. H., Hassanzadeh, S., and Hakkarainen, M. (2015). "Valorization of cellulose and waste paper to graphene oxide quantum dots," *RSC Adv.* 5(34), 26550-26558. DOI: 10.1039/C5RA01805F

Akar, E., Altınışık, A., and Seki, Y. (2012). "Preparation of pH-and ionic-strength responsive biodegradable fumaric acid crosslinked carboxymethyl cellulose," *Carbohydr. Polym*. 90(4), 1634-1641. DOI: 10.1016/j.carbpol.2012.07.043

Akhtar, M. F., Hanif, M., and Ranjha, N. M. (2016). "Methods of synthesis of hydrogels. A review," *Saudi Pharm J*. 24(5), 554-559. DOI: 10.1016/j.jsps.2015.03.022

An, L., Chen, J., Heo, J. W., Bae, J. H., Jeong, H., and Kim, Y. S. (2021a). "Synthesis of lignin-modified cellulose nanocrystals with antioxidant activity via Diels–Alder reaction and its application in carboxymethyl cellulose film," *Carbohydr. Polym*. 274, article 118651. DOI: 10.1016/j.carbpol.2021.118651

An, L., Si, C., Bae, J. H., Jeong, H., and Kim, Y. S. (2020). "One-step silanization and amination of lignin and its adsorption of Congo red and Cu (II) ions in aqueous solution," *Int. J. Biol. Macromol.* 159, 222-230. DOI: 10.1016/j.ijbiomac.2020.05.072

An, L., Yu, Y. H., Chen, J., Bae, J. H., Youn, D. H., Jeong, H. M., and Kim, Y. S. (2021b). "Synthesis and characterization of tailor-made zwitterionic lignin for resistance to protein adsorption," *Ind. Crops Prod.* 167, article 113514. DOI: 10.1016/j.indcrop.2021.113514

Bañuls-Ciscar, J., Abel, M.-L., and Watts, J. F. (2016). "Characterisation of cellulose and hardwood organosolv lignin reference materials by XPS," *Surf. Sci. Spectra* 23(1), 1-8. DOI: 10.1116/1.4943099

Brizzolara, D., Cantow, H.-J., Diederichs, K., Keller, E., and Domb, A. J. (1996). "Mechanism of the stereocomplex formation between enantiomeric poly(lactide)s," *Macromol.* 29(1), 191-197. DOI: 10.1021/ma951144e

Carafa, M., Marianecci, C., Di Marzio, L., Rinaldi, F., Di Meo, C., Matricardi, P., Alhaique, F., and Coviello, T. (2011). "A new vesicle-loaded hydrogel system suitable for topical applications: preparation and characterization," *J. Pharm. Pharm. Sci.* 14(3), 336-346. DOI: 10.18433/j3160b

Chatterjee, S., Lee, M. W., and Woo, S. H. (2010). "Adsorption of congo red by chitosan hydrogel beads impregnated with carbon nanotubes," *Bioresource Technol.* 101(6), 1800-1806. DOI: 10.1016/j.biortech.2009.10.051

Chen, J., Fan, X., Zhang, L., Chen, X., Sun, S., and Sun, R. C. (2020). "Research progress in lignin-based slow/controlled release fertilizer," *ChemSusChem* 13(17), 4356-4366. DOI: 10.1002/cssc.202000455

Chen, X., Liu, J., Lin, J., and Hong, J. (2016). "Study on the performance of cold-recycling asphalt mixture influenced by activity sites of lignin via chemical analysis," *J. Test. Eval.* 44(1), 498-506. DOI: 10.1520/JTE20140404

Chung, H. J., and Park, T. G. (2009). "Self-assembled and nanostructured hydrogels for drug delivery and tissue engineering," *Nano Today* 4(5), 429-437. DOI: 10.1016/j.nantod.2009.08.008

Ciolacu, D., and Cazacu, G. (2018). "New green hydrogels based on lignin," *J. Nanosci. Nanotechnol.* 18(4), 2811-2822. DOI: 10.1166/jnn.2018.14290

Ciolacu, D., Oprea, A. M., Anghel, N., Cazacu, G., and Cazacu, M. (2012). "New cellulose–lignin hydrogels and their application in controlled release of polyphenols," *Mater. Sci. Eng. C.* 32(3), 452-463. DOI: 10.1016/j.msec.2011.11.018

Cortés-Triviño, E., Valencia, C., Delgado, M. A., and Franco, J. M. (2018). "Modification of alkali lignin with poly (ethylene glycol) diglycidyl ether to be used as a thickener in bio-lubricant formulations," *Polym. J.* 10(6), 670. DOI: 10.3390/polym10060670

Cui, H., Zhuang, X., He, C., Wei, Y., and Chen, X. (2015). "High performance and reversible ionic polypeptide hydrogel based on charge-driven assembly for biomedical applications." *Acta biomater* 11, 183-190. DOI: 10.1016/j.actbio.2014.09.017

Dai, L., Ma, M., Xu, J., Si, C., Wang, X., Liu, Z., and Ni, Y. (2020). "All-lignin-based hydrogel with fast pH-stimuli responsiveness for mechanical switching and actuation," *Chem Mater.* 32(10), 4324-4330. DOI: 10.1021/acs.chemmater.0c01198

Dankers, P. Y., Harmsen, M. C., Brouwer, L. A., Van Luyn, M. J., and Meijer, E. (2005). "A modular and supramolecular approach to bioactive scaffolds for tissue engineering," *Nat. Mater*. 4(7), 568-574. DOI: 10.1038/nmat1418

Deng, J., He, Q., Wu, Z., and Yang, W. (2008). "Using glycidyl methacrylate as cross-linking agent to prepare thermosensitive hydrogels by a novel one-step method."*J. Polym. SCI., Part A: Polym. Chem.* 46(6), 2193-2201. DOI: 10.1002/pola.22554

Dinu, M. V., and Dragan, E. S. (2010). "Evaluation of Cu^{2+}, Co^{2+} and Ni^{2+} ions removal from aqueous solution using a novel chitosan/clinoptilolite composite: Kinetics and isotherms," *J. Chem. Eng.* 160(1), 157-163. DOI: 10.1016/j.cej.2010.03.029

Fan, X.-M., Yu, H.-Y., Wang, D.-C., Mao, Z.-H., Yao, J., and Tam, K.C. (2019). "Facile and green synthesis of carboxylated cellulose nanocrystals as efficient adsorbents in wastewater treatments," *ACS Sustain. Chem. Eng.* 7(21), 18067-18075. DOI: 10.1021/acssuschemeng.9b05081

Gennen, S., Grignard, B., Thomassin, J.-M., Gilbert, B., Vertruyen, B., Jerome, C., and Detrembleur, C. (2016). "Polyhydroxyurethane hydrogels: Synthesis and characterizations," *Eur. Polym. J.* 84, 849-862. DOI: 10.1016/j.eurpolymj.2016.07.013

Guo, K., Gao, B., Yue, Q., Xu, X., Li, R., and Shen, X. (2018). "Characterization and performance of a novel lignin-based flocculant for the treatment of dye wastewater," *Int. Biodeterior. Biodegrad.* 133, 99-107. DOI: 10.1016/j.ibiod.2018.06.015

Han, X., Zhang, Y., Ran, F., Li, C., Dai, L., Li, H., Yu, F., Zheng, C., and Si, C. (2022). "Lignin nanoparticles for hydrogel-based pressure sensor," *Ind. Crops Prod.* 176, article 114366. DOI: 10.1016/j.indcrop.2021.114366

Heo, J. W., An, L., Chen, J., Bae, J. H., and Kim, Y. S. (2022). "Preparation of amine-functionalized lignins for the selective adsorption of methylene blue and Congo red," *Chemosphere* 295, article 133815. DOI: 10.1016/j.chemosphere.2022.133815

Heo, J. W., Chen, J., Kim, M. S., Kim, J. W., Zhang, Z., Jeong, H., and Kim, Y. S. (2023). "Eco-friendly and facile preparation of chitosan-based biofilms of novel acetoacetylated lignin for antioxidant and UV-shielding properties," *Int. J. Biol. Macromol.* 225, 1384-1393. DOI: 10.1016/j.ijbiomac.2022.11.196

Jiang, B., Yao, Y., Liang, Z., Gao, J., Chen, G., Xia, Q., and Hu, L. (2020). "Lignin-based direct ink printed structural scaffolds."*Small*. 16(31), 1907212. DOI: 10.1002/smll.201907212

Li, B., Zhong, Q., Li, D., Xu, K., Zhang, L., and Wang, J. (2018). "Influence of ethylene glycol methacrylate to the hydration and transition behaviors of thermo-responsive interpenetrating polymeric network hydrogels," *Polym. J.* 10(2), 128. DOI: 10.3390/polym10020128

Lim, L. S., Rosli, N. A., Ahmad, I., Mat Lazim, A., and Mohd Amin, M. C. I. (2017). "Synthesis and swelling behavior of pH-sensitive semi-IPN superabsorbent hydrogels based on poly (acrylic acid) reinforced with cellulose nanocrystals," *Nanomaterials* 7(11), article 399. DOI: 10.3390/nano7110399

Lin, F., Zheng, J., Guo, W., Zhu, Z., Wang, Z., Dong, B., and Lu, B. (2019). "Smart cellulose-derived magnetic hydrogel with rapid swelling and deswelling properties for remotely controlled drug release," *Cellulose*. 26, 6861-6877. DOI: 10.1007/s10570-019-02572-0

Liu, T., Ren, X., Zhang, J., Liu, J., Ou, R., Guo, C., Yu, X., Wang, Q., and Liu, Z. (2020). "Highly compressible lignin hydrogel electrolytes via double-crosslinked strategy for superior foldable supercapacitors," *J. Power Sources* 449, 227532. DOI: 10.1016/j.jpowsour.2019.227532

Lv, Z., Zheng, Y., Zhou, H., Pan, Z., Li, C., Dai, L., Zhang, M., and Si, C. (2022). "Hydrothermal method-assisted synthesis of self-crosslinked all-lignin-based hydrogels," *Int. J. Biol. Macromol.* 216, 670-675. DOI: 10.1016/j.ijbiomac.2022.07.003

Madl, C. M., Katz, L. M., and Heilshorn, S. C. (2016). "Bio-orthogonally crosslinked,

engineered protein hydrogels with tunable mechanics and biochemistry for cell encapsulation." *Adv. Funct. Mater.* 26(21), 3612-3620. DOI: 10.1002/adfm.201505329

Mahmud, M., Daik, R. U. S. L. I., and Adam, Z. A. I. N. A. H. (2018). "Influence of poly (ethylene glycol) on the characteristics of γ radiation-crosslinked poly (vinyl pyrrolidone)-low molecular weight chitosan network hydrogels," *Sains Malays.* 47(6), 1189-1197. DOI: 10.17576/jsm-2018-4706-14

Majcher, M. J., McInnis, C. L., Himbert, S., Alsop, R. J., Kinio, D., Bleuel, M., and Hoare, T. (2020). "Photopolymerized starchstarch nanoparticle (SNP) network hydrogels." *Carbohydr. Polym*. 236, article 115998. DOI: 10.1016/j.carbpol.2020.115998

Mao, Y., Pan, M., Yang, H., Lin, X., and Yang, L. (2020). "Injectable hydrogel wound dressing based on strontium ion cross-linked starch," *Front. Mater. Sci*. 14, 232-241. DOI: 10.1007/s11706-020-0508-6

Meng, Y., Lu, J., Cheng, Y., Li, Q., and Wang, H. (2019). "Lignin-based hydrogels: A review of preparation, properties, and application," *Int. J. Biol. Macromol.* 135, 1006-1019. DOI: 10.1016/j.ijbiomac.2019.05.198

Morales, A., Labidi, J., and Gullón, P. (2020). "Assessment of green approaches for the synthesis of physically crosslinked lignin hydrogels," *Ind. Eng. Chem*. 81, 475-487. DOI: 10.1016/j.jiec.2019.09.037

Murakami, K., Aoki, H., Nakamura, S., Nakamura, S. I., Takikawa, M., Hanzawa, M., and Ishihara, M. (2010). "Hydrogel blends of chitin/chitosan, fucoidan and alginate as healing-impaired wound dressings," *Biomater* 31(1), 83-90. DOI: 10.1016/j.biomaterials.2009.09.031

Nguyen, N. T., Milani, A. H., Jennings, J., Adlam, D. J., Freemont, A. J., Hoyland, J. A., and Saunders, B. R. (2019). "Highly compressive and stretchable poly (ethylene glycol) based hydrogels synthesised using pH-responsive nanogels without free-radical chemistry," *Nanoscale*. 11(16), 7921-7930. DOI: 10.1039/C9NR01535C

Nguyen, H. T., Ngwabebhoh, F. A., Saha, N., Saha, T., and Saha, P. (2022). "Gellan gum/bacterial cellulose hydrogel crosslinked with citric acid as an eco-friendly green adsorbent for safranin and crystal violet dye removal," *Int. J. Bio. Macromol.* 222, 77-89. DOI: 10.1016/j.ijbiomac.2022.09.040

Olusegun, S. J., and Mohallem, N. D. (2020). "Comparative adsorption mechanism of doxycycline and Congo red using synthesized kaolinite supported $CoFe_2O_4$ nanoparticles," *Environ Pollut.* 260, article 114019. DOI: 10.1016/j.envpol.2020.114019

Passauer, L. (2012). "Highly swellable lignin hydrogels: Novel materials with interesting properties," in: *Functional Materials from Renewable Sources*, J. Am. Chem. Soc., pp. 211-228.

Peppas, N. A., Bures, P., Leobandung, W., and Ichikawa, H. (2000). "Hydrogels in pharmaceutical formulations," *Eur. J. Pharm. Biopharm.* 50(1), 27-46. DOI: 10.1016/s0939-6411(00)00090-4

Piccinino, D., Capecchi, E., Tomaino, E., Gabellone, S., Gigli, V., Avitabile, D., and Saladino, R. (2021). "Nano-structured lignin as green antioxidant and UV shielding ingredient for sunscreen applications," *Antioxidants* 10(2), article 274. DOI: 10.3390/antiox10020274

Ragauskas, A. J., Beckham, G. T., Biddy, M. J., Chandra, R., Chen, F., Davis, M. F., and Wyman, C. E. (2014). "Lignin valorization: improving lignin processing in the

biorefinery," *Science*. 344(6185), article 1246843. DOI: 10.1126/science.1246843

Rico-García, D., Ruiz-Rubio, L., Pérez-Alvarez, L., Hernández-Olmos, S.L., Guerrero-Ramírez, G. L., and Vilas-Vilela, J. L. (2020). "Lignin-based hydrogels: Synthesis and applications," *Polym. J.* 12(1), 81. DOI: 10.3390/polym12010081

Scarica, C., Suriano, R., Levi, M., Turri, S., and Griffini, G. (2018). "Lignin functionalized with succinic anhydride as building block for biobased thermosetting polyester coatings," *ACS Sustain. Chem. Eng.* 6(3), 3392-3401. DOI: 10.1021/acssuschemeng.7b03583

Sharma, S., and Tiwari, S. (2020). "A review on biomacromolecular hydrogel classification and its applications," *Int. J. Biol. Macromol.* 162, 737-747. DOI: 10.1016/j.ijbiomac.2020.06.110

Sheng, Y., Ma, Z., Wang, X., and Han, Y. (2022). "Ethanol organosolv lignin from different agricultural residues: Toward basic structural units and antioxidant activity," *Food Chem.* 376, article 131895. DOI: 10.1016/j.foodchem.2021.131895

Shim, W. S., Yoo, J.S., Bae, Y. H., and Lee, D. S. (2005). "Novel injectable pH and temperature sensitive block copolymer hydrogel," *Biomacromolecules* 6(6), 2930-2934. DOI: 10.1021/bm050521k

Teng, X., Xu, H., Song, W., Shi, J., Xin, J., Hiscox, W.C., and Zhang, J. (2017). "Preparation and properties of hydrogels based on PEGylated lignosulfonate amine," *ACS Omega* 2(1), 251-259. DOI: 10.1021/acsomega.6b00296

Thakur, V. K., and Thakur, M. K. (2015). "Recent advances in green hydrogels from lignin: a review," *Int. J. Biol. Macromol.* 72, 834-847. DOI: 10.1016/j.ijbiomac.2014.09.044

Tian, R., Liu, Q., Zhang, W., and Zhang, Y. (2018). "Preparation of lignin-based hydrogel and its adsorption of Cu^{2+} ions and Co^{2+} ions in wastewaters," *J. Inorg. Organomet. Polym. Mater*. 28, 2545-2553. DOI: 10.1007/s10904-018-0943-3

Truong, T. T. C., Vo, N. T. T., Nguyen, K. D., and Bui, H. M. (2019). "Preparation of cellulose-based hydrogel derived from tea residue for the adsorption of methylene blue." *Cell Chem. Technol*. 53, 573-582. DOI: 10.35812/CelluloseChemTechnol.2019.53.57

Wang, X., Zhang, Y., Hao, C., Dai, X., Zhou, Z., and Si, N. (2014). "Ultrasonic-assisted synthesis of aminated lignin by a Mannich reaction and its decolorizing properties for anionic azo-dyes," *RSC Adv.* 4(53), 28156-28164. DOI: 10.1039/c4ra03133d

Yoo, C. J., Narayanan, P., and Jones, C. W. (2019). "Self-supported branched poly (ethyleneimine) materials for CO_2 adsorption from simulated flue gas," *J. Mater. Chem. A* 7, 19513-19521. DOI: 10.1039/C9TA04662C

You, X., Gu, Z., Huang, J., Kang, Y., Chu, C. C., and Wu, J. (2018). "Arginine-based poly (ester amide) nanoparticle platform: From structure–property relationship to nucleic acid delivery," *Acta Biomater* 74, 180-191. DOI: 10.1016/j.actbio.2018.05.040

Yue, X., Chen, F., and Zhou, X. (2011). "Improved interfacial bonding of PVC/wood-flour composites by lignin amine modification," *BioResources* 6(2), 2022-2044.

Zainal, S. H., Mohd, N. H., Suhaili, N., Anuar, F. H., Lazim, A. M., and Othaman, R. (2021). "Preparation of cellulose-based hydrogel: A review." *JMR&T*. 10, 935-952. DOI: 10.1016/j.jmrt.2020.12.012

Zerpa, A., Pakzad, L., and Fatehi, P. (2018). "Hardwood kraft lignin-based hydrogels: Production and performance," *ACS Omega* 3(7), 8233-8242. DOI: 10.1021/acsomega.8b01176

Zhang, J., Lin, X., Luo, X., Zhang, C., and Zhu, H. (2011). "A modified lignin adsorbent for the removal of 2, 4, 6-trinitrotoluene," *J. Chem. Eng.* 168(3), 1055-1063. DOI: 10.1016/j.cej.2011.01.083

Zhang, Z., Li, F., Heo, J. W., Chen, J., Kim, J. W., Kim, M. S., and Kim, Y. S. (2023a). "N-Hydroxysuccinimide-catalyzed facile synthesis of high-phenolic-hydroxyl-content lignin for enhanced antioxidant properties," *J. Wood Chem. Technol.* 43(1), 35-45. DOI: 10.1080/02773813.2023.2173781

Zhang, Z., Li, F., Heo, J. W., Kim, J. W., Kim, M. S., Xia, Q., and Kim, Y. S. (2023b). "Decoration of sodium carboxymethylcellulose gel microspheres with modified lignin to enhanced methylene blue removal," *Int. J. Biol. Macromol.* 242, article 125041. DOI: 10.1016/j.ijbiomac.2023.125041

Zhang, Z., Li, F., Heo, J. W., Kim, J. W., Kim, M. S., Xia, Q., and Kim, Y. S. (2023). "Facile synthesis of phenolic hydroxyl-rich modified lignin: Evaluation of their applications as an antioxidant and for Cr (VI) removal," *Ind. Crop. Prod*. 205, article 117403. DOI: 0.1016/j.indcrop.2023.117403

Zheng, Y., Huang, K., You, X., Huang, B., Wu, J., and Gu, Z. (2017). "Hybrid hydrogels with high strength and biocompatibility for bone regeneration," *Int. J. Biol. Macromol.* 104, 1143-1149. DOI: 10.1016/j.ijbiomac.2017.07.017

Article submitted: March 7, 2024; Peer review completed: May 5, 2024; Revised version received and accepted: June 12, 2024: Published: June 19, 2024.
DOI: 10.15376/biores.19.3.5316-5337

APPENDIX: SUPPLEMENTARY DATA

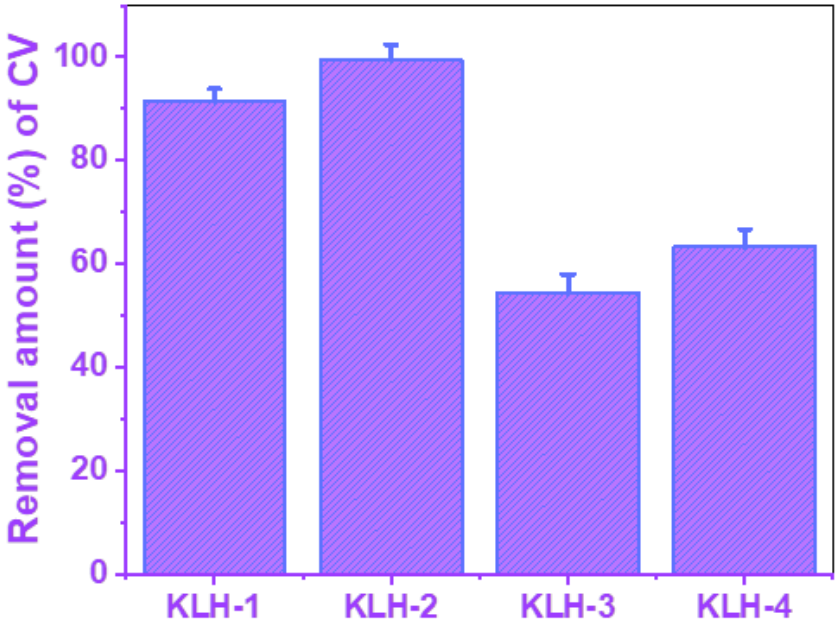

Fig. S1. Effect of KLH samples on the removal efficiency of CV